The Interplay between Surface Plasmon Resonance and Switching Properties in Gold@Spin Crossover Nanocomposites

Marlène Palluel, Ngoc Minh M Tran, Nathalie Daro, Sonia Buffiere, Stéphane Mornet, Eric Freysz, Guillaume Chastanet

WILEY-VCH

DOI: 10.1002/ ((please add manuscript number))
Article type: Full Paper

The Interplay between Surface Plasmon Resonance and Switching Properties in Gold@Spin Crossover Nano-Composites

Marlène Palluel, Ngoc Minh Tran, Nathalie Daro, Sonia Buffière, Stéphane Mornet,* Eric Freysz* and Guillaume Chastanet*

M. Palluel, Dr. N. Daro, Dr. S. Mornet, S. Buffière, Dr. G. Chastanet
CNRS, Univ. Bordeaux, ICMCB, UMR 5026, 87 Avenue du Dr A. Schweitzer, F-33608 Pessac, France.
E-mail: guillaume.chastanet@icmcb.cnrs.fr; stephane.mornet@icmcb.cnrs.fr
Dr. N. M. Tran, Dr. E. Freysz
Univ. Bordeaux, CNRS, UMR 5798, LOMA, 358 Cours de la libération, F-33405 Talence cedex, France.
E-mail: eric.freysz@u-bordeaux.fr

Keywords: Spin crossover, surface plasmon resonance, gold nanoparticle, photoswitching, SPR modulation.

Abstract: Rod-like gold nanoparticles were directly embedded in a 1D-polymeric Spin CrossOver (SCO) material leading to singular Au@SCO nanohybrid architectures. The resulting architectures are designed to promote a synergetic effect between ultrafast spin-state photoswitching and photothermal properties of plasmonic nanoparticles. This synergy has been evidenced by the strong modulation of the surface plasmon resonance of the gold nanorods through the spin-state switching of the SCO component and also the strong enhancement of the photoswitching efficiency compared to pure SCO particles. This remarkable synergy results from the large modulation of the dielectric properties of the SCO polymer upon its thermal switching and the enhancement of the heating of these hybrid nanostructures upon excitation of the surface plasmon resonance of the gold nanorods.

1. Introduction

Spin CrossOver (SCO) is a versatile switching phenomenon that results in remarkable changes in magnetic, optical and mechanical properties of materials upon external perturbation such as light, temperature or pressure[1]. Molecular-based SCO compounds offer many interesting prospects in molecular electronics.[2] Along this line, lots of efforts have been devoted to synthesize and design SCO nanoparticles (NPs)[3,4] with controlled shape and size. Among SCO materials that can be processed at the nanometer scale, while keeping the properties they exhibit at the macroscopic scale, the attention has been driven towards polymeric triazol based iron(II) complexes. Thanks to an appropriate tuning of ligands and anions, these complexes can exhibit a large thermal hysteresis loop between a high spin (HS) and a low spin (LS) state of iron(II) centred at room temperature[5]. Such a hysteresis loop makes it possible to record and store information in such compounds. The recording can be induced by different means. For instance, it has been demonstrated that fast photoswitching can be recorded using nanosecond laser pulses which central wavelength is centred around the iron(II) *d-d* or metal to ligand charge transfer (MLCT) absorption bands of the complex.[6,7] Upon excitation, the sample, initially set within its thermal hysteresis loop and in the LS state, is heated and driven to the HS state. The heating of the compound induced by the laser pulse can be of several degrees according to the laser fluence and the switching time depends on its size. Hence, the photoswitching time of the NPs was demonstrated to be drastically reduced.[7]

The controlled synthesis of SCO nanomaterials makes it possible to introduce many other functionalities. For instance, coating the SCO particles with silica offers a platform to graft new functions at their surfaces, such as luminescent molecules[8] or gold nanoparticles (AuNPs).[9] Combining the properties of SCO materials and AuNPs has been shown to open promising properties, in particular because these metal nanoparticles display photothermal heating properties in the visible and near-infrared range resulting from the non-radiative decay of localized surface plasmons. For instance, it has been demonstrated that exciting the

plasmon resonance of 14 nm spherical AuNPs reduces significantly the power required to photoswitch SCO complexes.[9] In this architecture, upon excitation of the plasmon resonance, AuNPs act as efficient local nano heaters.[10] For such designed AuNPs-SCO nano ensemble, a four-time reduction of the photoswitching laser intensity was demonstrated. To further improve the heat transfer from the AuNPs to the SCO NPs avoiding the silica interphase, we have recently reported a direct grafting of gold nanospheres onto SCO nanoparticles. Following this approach, a well-controlled amount of gold nanospheres of various sizes were grafted on $[Fe(Htrz)_2(trz)](BF_4)$ (Htrz = 1*H*-1,2,4-triazole and trz = deprotonated triazolato(-) ligand) nanoparticles.[11]

To further reduce the laser fluence and switching time required to photoswitch AuNPs-SCO nanoensemble hereafter, we propose another approach. It consists of a direct coating of gold nanorods (AuNRs) by SCO material. AuNRs are of particular interest since they exhibit a broad longitudinal surface plasmon resonance (SPR) band centred in the near-infrared,[10] a spectral region where the SCO in the LS state is almost transparent. It is noteworthy to mention that directly coating of AuNRs with SCO will improve the contact and therefore the heat diffusion among the metallic particles (*i.e.* AuNRs) and the SCO complexes. This is shown to drastically enhance the plasmonic assisted photoswitching of the as-prepared nanocomposites.

Hereafter, we report on the coating of AuNRs by the 1D-polymeric iron(II) compound of formula $[Fe(Htrz)_2(trz)](BF_4)$.[4f] This original procedure was achieved developing a direct coating of the AuNRs by the SCO compound. The latter is shown to be highly reproducible. The Au@SCO NRs exhibit a widening of the thermal hysteresis loop compared to the pure SCO NPs. Moreover, a drastic reduction of the laser fluence required to photoswitch the nanocomposites is recorded. Furthermore, we evidence a large shift of the plasmon resonance of the AuNRs upon switching of the SCO complex. This ensemble of results demonstrates the interplay between the SCO phenomenon and the SPR of these original core-shell NPs.

2. Results and Discussions

2.1. Methodology

At first, we explore the conditions under which the crucial stability of the colloidal suspensions of the synthesized AuNRs[12] is kept during coating them with the 1D-$[Fe(Htrz)_2(trz)](BF_4)$ compound. Second addresses the direct synthesis of the nanocomposites through the polymerization of the $[Fe(Htrz)_2(trz)](BF_4)$ chain around the AuNRs. To ensure that a large number of SCO NPs contains at least one AuNR, we explore several reactants' concentrations. $[Fe(Htrz)_2(trz)](BF_4)$ nanoparticles without AuNRs are prepared as well. This makes it possible to compare the crystalline phase of the SCO shell, as well as the switching properties, with a reference compound. The latter is prepared using either a well-described reverse-micellar protocol [4f] or a direct synthesis approach detailed below.

2.2. Synthesis and stability of gold nanorods

The AuNRs are synthesized according to the well-known and highly reproducible seed-growth method (**Figure S1**).[12] From the TEM images, the dimensions of these NRs are estimated through a normal law fit of the histograms (Figure SI1b) to be 60 ± 8 nm for the length and 15 ± 4 nm for the width. Accordingly, the mean value of the aspect ratio is 4 ± 2. The UV-visible spectrum of this colloidal suspension (**Figure 1**) exhibits an intense and large absorption band at 780 nm associated to the longitudinal SPR mode of the AuNRs and an additional band at 540 nm associated to the transverse mode.[10]

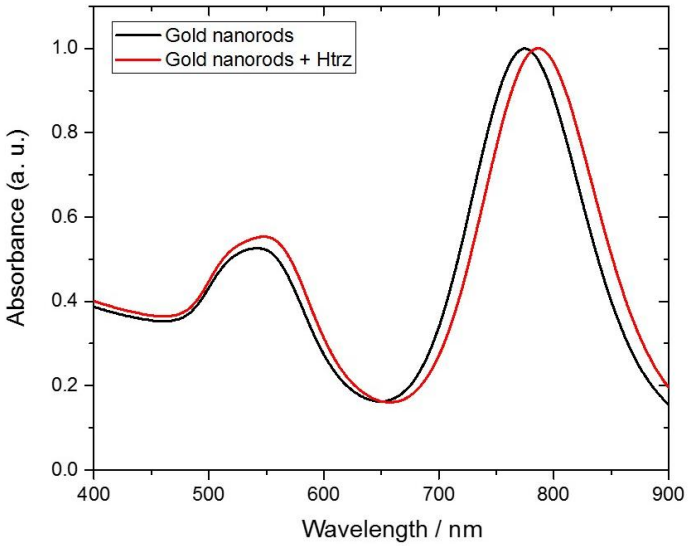

Figure 1: Absorption spectra of gold nanorods dispersion in water, stabilized by 5 mM of CTAB, before (black curve) and after addition of 1.8 M of Htrz ligand aqueous solution. (Nota: the concentration of 1.8 M is further used for the synthesis of the nanocomposites).

It is noteworthy to mention that the direct synthesis of the SCO compound is performed by adding an aqueous solution of $Fe(BF_4)_2$ into a alcoholic solution of 1H-1,2,4-triazole (Htrz), at room temperature.[13] However, the AuNRs dispersion, which is stable in CTAB (5 mM) aqueous solution, becomes unstable into a hydro-alcoholic mixture and in the presence of $Fe(BF_4)_2$. Therefore, we test the stability of the AuNRs suspension in different water/ethanol ratios (100/0, 80/20, 60/40, 40/60, 20/80). These tests are performed monitoring the color change of the AuNRs dispersion. Indeed, the stable dispersion has a burgundy color whereas, when destabilized, the colloidal dispersion flocculates as a black powder (**Figure SI2**). This allows us to infer an optimum water/ethanol ratio of 60/40. Above 40 % of ethanol, the outer layer of the CTAB shell around the AuNRs is likely transferred into the solution, destabilizing the colloidal suspension.

In this study, we hypothesize that the amphiphilic Htrz ligands partially exchange the outer layer of CTAB around the AuNRs,[11] enabling the colloidal stability during the SCO growth. Therefore, different concentrations and volumes of Htrz solutions are tested. The stability of the AuNRs suspension is examined immediately after adding the Htrz, after 1 hour

and 24 hours of absorption time. Up to 2 M of Htrz the dispersion remains stable below 40 % of ethanol, even after 24 hours (**Table SI1**) while above this ratio, the suspension is destabilized (**Table SI2 and SI3 and Figure SI3**).

The UV-Vis spectrum of the aqueous dispersion of AuNRs with 1.8 M of Htrz shows a clear change in the position of the absorption bands (Figure 1). Upon addition of Htrz, the band at 780 nm is red-shifted to 788 nm, indicating an 8 nm shift of the longitudinal SPR mode. It is worth mentioning that the redshift of the transverse mode is weaker and about 5 nm.

Hence, the spectral shift of the SPR bands displayed in Figure 1 is in agreement with previously reported work[11] and the assumption we made above: Htrz partially exchanges the outer layer of CTAB. However, one cannot precisely indicate the level of substitution. The interesting processes occurring at the interface of the AuNRs in presence of Htrz deserve a complete study, out of the scope of this current work. In consequence, we decided to perform the synthesis of the composite materials using a solvent mixture of 40 % of ethanol and 60 % of water. Here also, above 40 % of ethanol, most of the outer layer of the CTAB around the AuNRs is removed. This might improve the interface between the gold surface and the SCO polymer in the nanocomposites.

2.3. Synthesis of the composite nanomaterials

The synthesis of the SCO NPs of $[Fe(Htrz)_2(trz)](BF_4)$ is a well-known process. $[Fe(Htrz)_2(trz)](BF_4)$ NPs mainly exhibit rod-like morphology. Perfect control of the size can be achieved following micellar methods.[4f,13,14] In this study, two different approaches are used to obtain reference $[Fe(Htrz)_2(trz)](BF_4)$ compounds, keeping the same reaction conditions (concentration of reactants and temperature). Particles **1** are synthesized at room temperature according to the micellar approach (compound **1**, **Figure 2**).[4f] Compound **2** is synthesized using the direct method. It consists in mixing solutions of $[Fe(BF_4)_2]$ (1.2 M) and

Htrz (3.6 M) in a 60:40 mixture of water and ethanol. This mixture is performed at room temperature.

The synthesis of the nanocomposites is undertaken following the direct method consisting in coating the AuNRs with the SCO polymer. A first synthesis is performed using the same conditions as for the synthesis of **2,** adding a solution of $[Fe(BF_4)_2]$ to the dispersion of the AuNRs previously mixed with Htrz ligand. After mixing and centrifugation a dark purple powder is obtained (compound **3**). The concentration of AuNRs in the colloidal dispersion ($7.3\ 10^{15}$ particles per liter for 20 mM of gold) is kept constant while decreasing the concentration of the SCO reactants from [Fe] = 0.4 M, compound **4** to [Fe] = 0.3 M, (compound **5**). Such dilution impacts the reaction yield, ranging from 38 % for **3** to 53 % for **5**. The most relevant characteristics of the different compounds synthesized are reported in **Table 1**. The size, morphology and switching properties of each of these compounds were analyzed and are discussed hereafter.

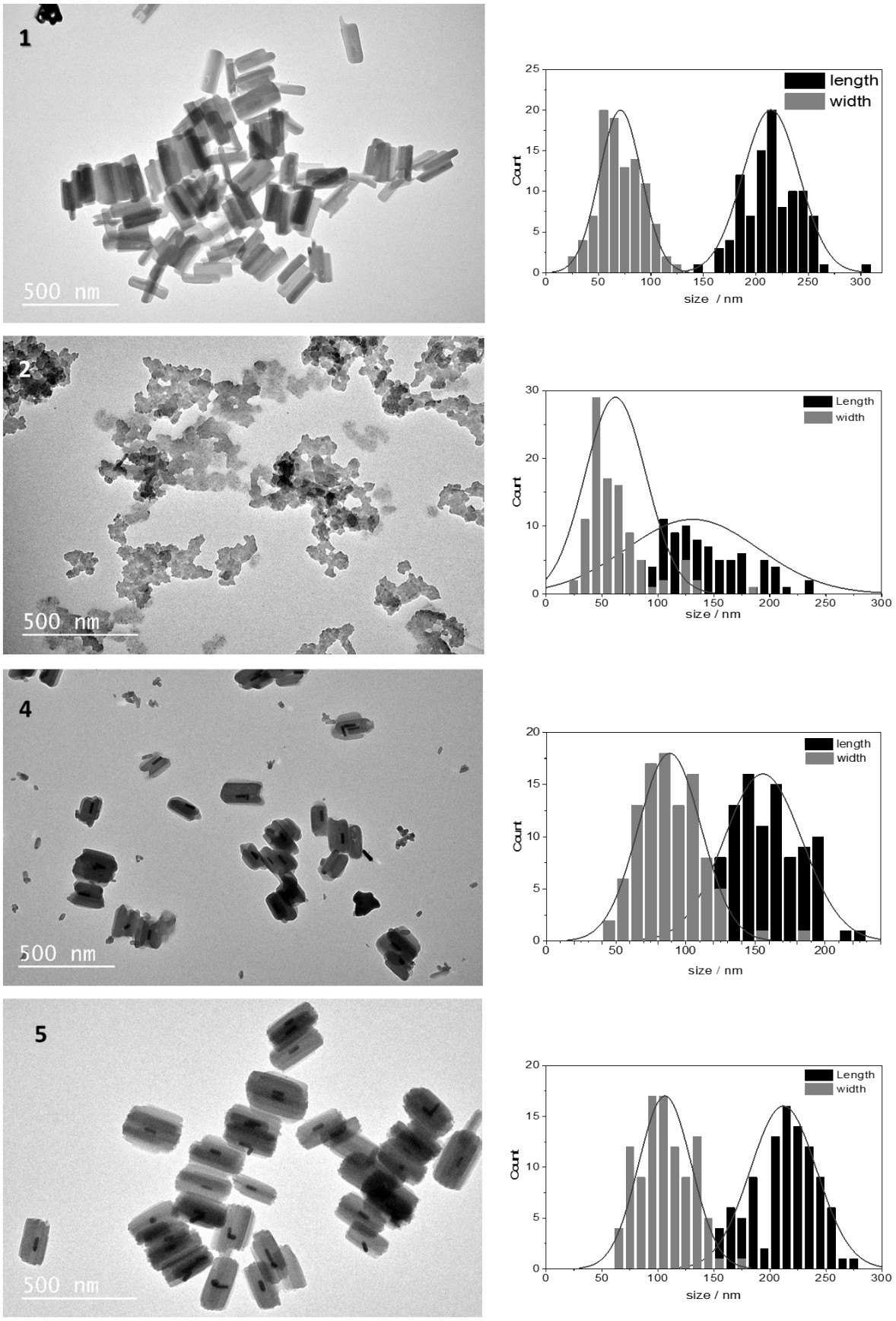

Figure 2: TEM images and size distributions of samples **1** ($[Fe(Htrz)_2(trz)](BF_4)$ obtained from micellar synthesis), **2** ($[Fe(Htrz)_2(trz)](BF_4)$ obtained from direct synthesis) and **4** and **5** ($Au@[Fe(Htrz)_2(trz)](BF_4)$).

	Compound	[Fe] (M)	Size (nm)	Polymorph	Filling[a]
1	SCO [b]	1.2	214 ± 27 x 71 ± 20	I	
2	SCO [c]	1.2	131 ± 59 x 62 ± 27	II	
3	Au@SCO [c]	1.2	< 200	II	< 10 %
4	Au@SCO D3 [c]	0.4	155 ± 28 x 88 ± 23	I	75 %
5	Au@SCO D4 [c]	0.3	212 ± 30 x 106 ± 24	I	90 %

a: ratio of SCO particles embedding at least one gold nanorod. *b*: NPs obtained by micellar synthesis. *c*: NPs obtained by direct method.

Table1: Summary of the studied compounds and their related characteristics.

2.4. Morphological characterization of nanomaterials by electron microscopy

Compounds **1-5** are first characterized by Transmission Electron Microscopy (TEM, **Figure 3** and **SI4**). Compound **1** consists of well-shaped and well-separated rods of 214 ± 27 nm x 71 ± 20 nm size, as expected for such synthesis (figure 2)[4f]. The TEM images for compounds **2** and **3** show poorly defined particles (figure 2 and SI4): the size is difficult to estimate, especially for **3** (below 200 nm). Table 1 indicates a large size distribution for compound **2**. Moreover, in compound **3**, very few AuNRs are present. Compounds **4** and **5** have well defined rod-like shape of 155 ± 28 nm by 88 ± 23 nm for compounds **4** and 212 ± 30 nm by 106 ± 24 nm for compound **5** (Figure 2). Several conclusions can be drawn from these images.

First, one can clearly see in the center of compounds **4** and **5** the presence of dark rods (about 60 nm long and 15 nm large) close to the dimensions of the AuNRs. Electron Dispersive Spectroscopy (EDS) analysis, performed on these nanoparticles (**Figure SI5**), clearly confirms that these dark NRs are indeed the AuNRs.

Second, from the TEM images, one can estimate that 75 to 90 % of the SCO particles are filled with at least one AuNR. This indicates the synthetic strategy we used is successful, making possible to produce more than 75 % of SCO coated AuNRs. The filling ratio (table 1) increases as [Fe] decreases. For most NPs, the AuNRs appear to be centred in a shell of $[Fe(Htrz)_2(trz)](BF_4)$. The thickness of the SCO shell is about 75 nm (**4**) and 50 nm (**5**) along the long axis and about 45 nm (**4**) and 35 nm (**5**) along the short axis. Assuming both gold and

Au@SCO composites are cylindrical, one can estimate that the AuNRs occupy less than 1% of the volume of the composites. Regarding the difference of density between the two compounds (19.3 g/cm^3 for gold and 1.9 g/cm^3 for the spin crossover compound[14a]), the AuNRs represent less than 10 % of the whole mass of the sample.

Third, the size of the particles is close to the ones obtained through the micellar synthesis (compound **1**). The latter will offer an important element of comparison when the properties are discussed. It has been previously shown that the decrease of iron(II) reactant is not expected to induce a better definition of size and shape on this compound.[15] Therefore the well-defined morphology observed in **4** and **5** may result from a templating effect induced by the presence of AuNRs. An interesting fact is that this possible templating effect also affects the 10 to 15 % of SCO particles that do not host AuNRs.

2.5. Structural characterization by X-ray powder diffraction

Powder X-ray diffraction (PXRD) is performed using capillary sample holders and compared to a reference of polymorph I.[4f,13] The PXRD patterns are reported in **Figure 3**. It appears clear that compounds **2** and **3** do not exhibit the same pattern that all the other compounds or the reference pattern. Indeed, instead of a doublet around 11°, a well-defined singlet is observed. Similarly, at 18° a large peak is observed instead of a clear doublet. Compounds **2** and **3** do not correspond to the expected phase and it could correspond to another already reported polymorph II.[13b] Below 30°, compounds **1**, **4** and **5** have the same features as the $[Fe(Htrz)_2(trz)](BF_4)$ reference spectrum. Two additional peaks on **4** and **5** can be seen at 38° and 45° (as well as on **3**). The latter corresponds to gold,[16] in agreement with the observations made from the TEM images. Hence we can conclude that these three compounds correspond to the targeted composite materials.

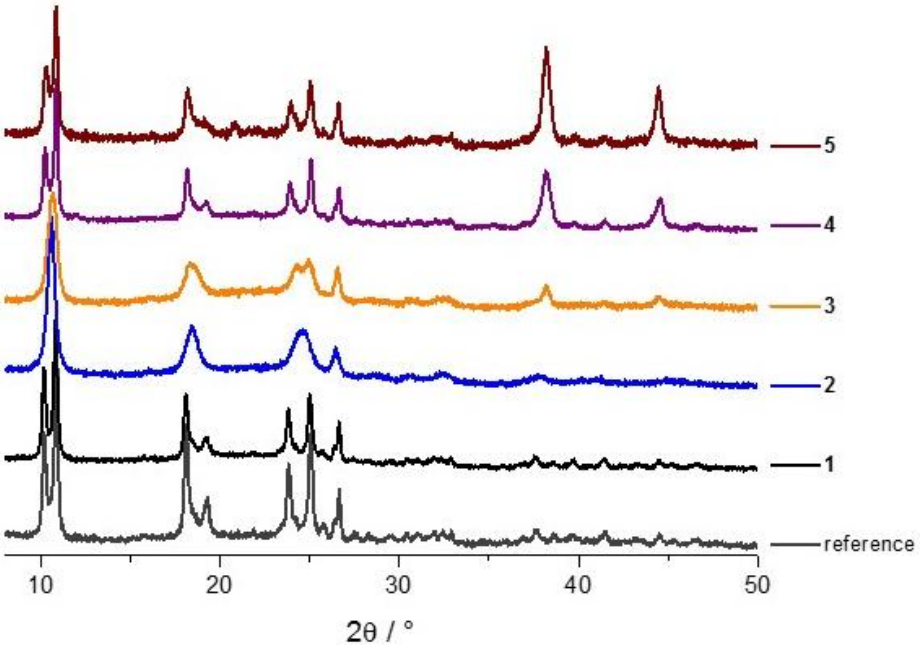

Figure 3: Powder X-Ray Diffraction patterns of compounds **1-5**, measured using capillary sample holders.

2.6. Evaluation of switching properties

The switching properties of these composite architectures are investigated by means of magnetic measurements using a SQUID magnetometer (**Figure 4**) and the related data are detailed in Table 2. The hysteresis cycles presented in Figure 4 relate to the stabilized cycles. Indeed, as already well documented for this compound, a first run-in step is needed to observe stable thermoswitching properties.[4f,13] All these compounds exhibit a $\chi_M T$ value at 390 K around 3.1 cm^3 K mol^{-1} (χ_M being the molar magnetic susceptibility), consistent with the HS, S = 2, configuration of the Fe(II) in the structure. Various widths of the hysteresis loop are observed (Table 2). Moreover, a HS residue of around 15 % at low temperature is recorded. This latter is in agreement with the behavior previously reported for such nanoparticles.[4f]

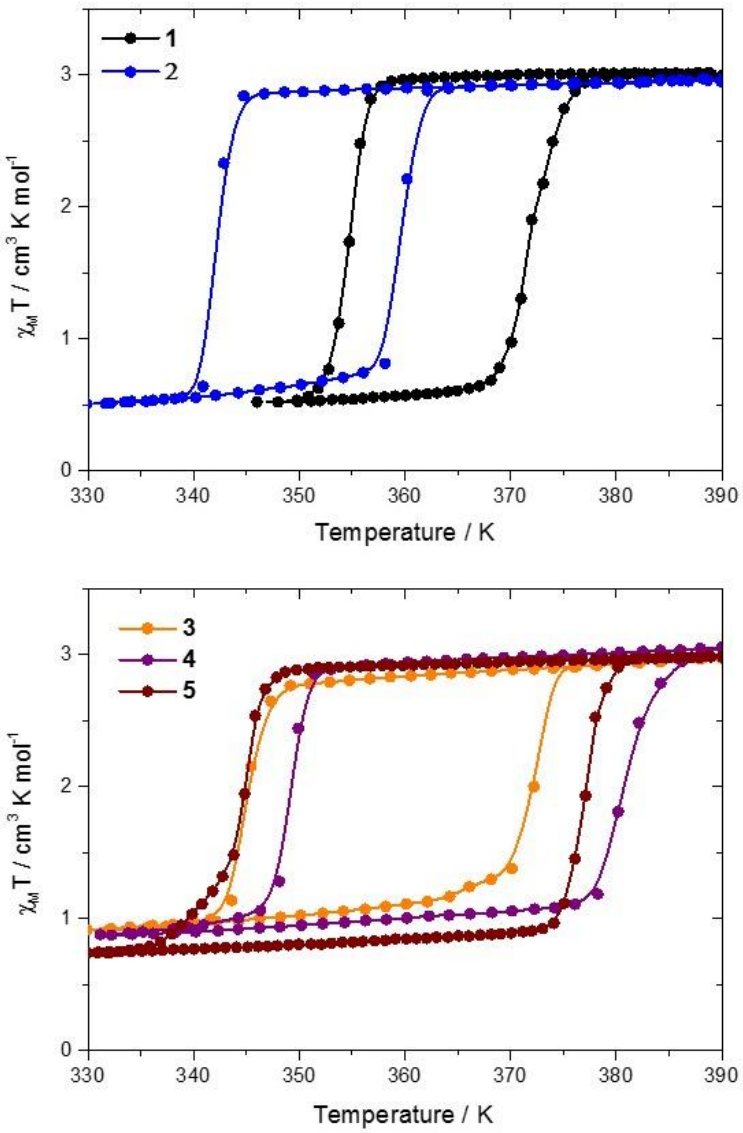

Figure 4: Thermal evolution of the $\chi_M T$ product of samples **1-5** at an applied magnetic field of 10 kOe and for a temperature sweep of 0.7 K/mn.

Compound **1** exhibits the classical hysteretic behavior of $[Fe(Htrz)_2(trz)](BF_4)$ nanoparticles with the switching temperature in warming mode $T_{1/2}\uparrow$ = 372 K and in cooling mode $T_{1/2}\downarrow$ = 355 K, leading to a 17 K thermal hysteresis width.[4f] Compound **2** exhibits a similar thermal hysteresis loop. However, compared to **1**, the latter is shifted by 12 K to lower temperatures. This shift is likely due to the fact that compound **2** does not belong to the same phase as compound **1** (cf. Table 1). Compounds **3-5** exhibit much wider thermal hysteresis loops

(Table 2), up to 33 K large for compound **5**. Comparing the compounds belonging to the same polymorph I (**1**, **4** and **5**), it seems that the thermal hysteresis width increases with the content of gold within the composite particles. Despite the fact that we have a mixture of neat SCO and nanocomposites in **4** and **5**, only a single hysteresis loop is recorded. Hence, besides the templating effect previously hypothesized in the microscopy analysis, the synthesis using AuNRs seems to broaden the thermal hysteresis loop of both neat SCO and composite nanoparticles present in compounds **4** and **5**, compared to compounds **1** and **2**. Accordingly, one can consider that the properties of the neat SCO particles present in **4** and **5** are identical to the ones of the nanocomposites.

	Compound	Size (nm)	Filling[a]	$T_{1/2}(\downarrow)$ (K)	$T_{1/2}(\uparrow)$ (K)	ΔT (K)[b]	% hυ
1	SCO	214 ± 27 x 71 ± 20		355	372	17	15
2	SCO	131 ± 59 x 62 ± 27		343	360	17	15
3	Au@SCO	< 200	< 10 %	345	372	27	0
4	Au@SCO	155 ± 28 x 88 ± 23	75 %	350	380	30	45
5	Au@SCO	212 ± 30 x 106 ± 24	90 %	342	376	34	55

a: ratio of SCO particles embedding at least one gold nanorod. *b:* $\Delta T = T_{1/2}(\uparrow) - T_{1/2}(\downarrow)$.

Table 2: Summary of the studied compounds and their switching features.

The thermo-induced switching of these compounds is also recorded by an optical mean performing optical spectroscopy. This is done on compounds **1** and **5**. The samples are prepared by sandwiching a very thin layer of powder in between two glass microscope coverslips. The experiments are carried out shining the sample with a broadband halogen light source and recording the spectra of the transmitted light with and without the sample with a compact spectrometer versus the temperature. The relative optical density is evaluated by computing the logarithmic ratio of the sample spectra over the reference spectra. **Figures SI6-**

7 and 5a report on the optical spectra of compounds **1, 4** and **5**, in the LS and HS states, respectively. According to these spectra, several observations can be made.

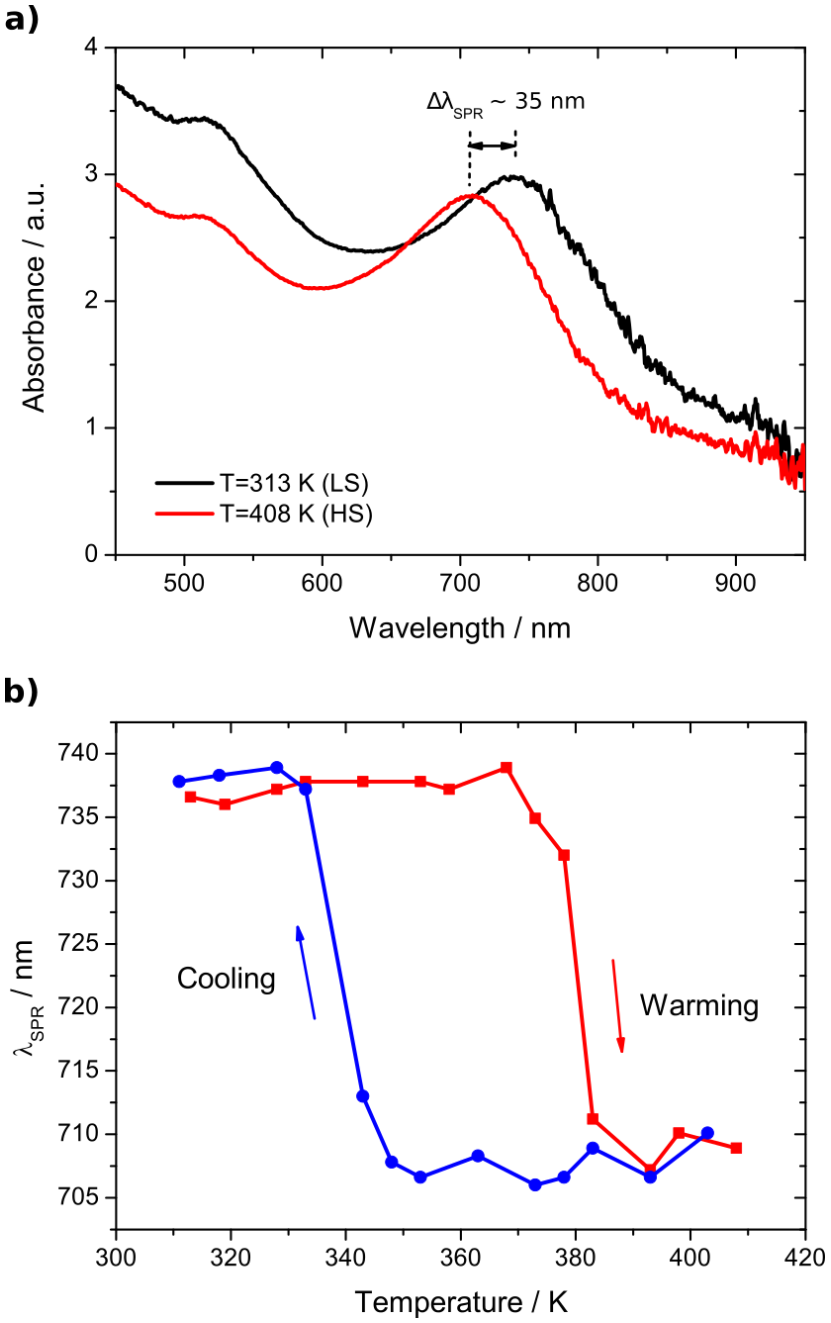

Figure 5: (a) Optical spectra of compound **5** recorded at 313 K and 408 K, respectively. (b) Evolution of the peak of SPR upon temperature variation in both warming and cooling mode.

First, at 313 K (black curve), the absorbance of the samples recorded below 600 nm is higher than the one recorded at 408 K (red curve). This phenomenon is likely due to the spin

crossover of the $[Fe(Htrz)_2(trz)](BF_4)$ component.[17] Indeed, the *d-d* transition of the Fe(II) in its LS state absorbs around 550 nm. Upon warming, this band disappears and the *d-d* transition of the Fe(II) in its HS state weakly grows around 830 nm. In Figure 5a, the growth of the "HS" band is likely hidden by the strong absorption peak of the gold particles.

Second, the SPR band in compound **5**, recorded at 313 K (40°C), is located at 740 nm. It is noteworthy to mention a 40 nm difference compared to the pure AuNRs spectrum in solution (Figure 1). This difference may rely on the fact that the AuNRs spectra are recorded in solution while the spectra of compounds **1** and **5** are recorded in the solid phase.

Third**,** the plasmon resonance band at 740 nm, recorded at 313 K when the SCO compound is LS (black curve), shifts towards 706 nm at 408 K (135 °C) when the SCO compound is HS (red curve). Note that there is no obvious spectral shift around the transverse plasmon resonance centred at 515 nm.

The shift of about 35 nm of the SPR band of the gold nanoparticle embedded in a SCO particle can be used to follow the spin crossover as a function of the temperature. Figure 5b reports the thermal evolution of the maximum of the surface plasmon resonance band both in warming and cooling modes, based on spectra recorded every 10 degrees. The plot indicates a sharp hysteresis curve with transition temperatures and width in agreement with the magnetic data.

The Au@SCO nanocomposites therefore present well-defined thermo-induced switching properties, with large hysteresis width. Moreover, the spin-state switching strongly impacts the SPR of the AuNR core since 35 nm of modulation is observed upon SCO. The increase of temperature cannot solely account for this strong variation of the SPR since a 17 nm of redshift is recorded when gold nanospheres are heated up by 1 000 degrees.[18] It is worth mentioning that this interplay between spin crossover and SPR is much stronger than the ones previously reported on related hybrid architectures.[19,20] The strong shift is related to the shift of the longitudinal SPR of AuNRs upon the change of the refractive index (or dielectric

function) of the medium surrounding the plasmonic surface.[21] As the SCO compounds have a higher refractive index in the LS state than in its HS state,[22] we do expect to record a blue shift of the AuNRs SPR upon switching from the LS to HS state of the SCO compound. Indeed it has previously been shown that the position of the longitudinal plasmon resonance λ_p scales as λ_p (nm) = $\alpha.\varepsilon_m$+ b where the constant α depends on the aspect ratio R of the AuNR, ε_m is the dielectric constant of the medium in which AuNRs are embedded and b is a constant.[21] In our case, for gold nanoparticles with an aspect ratio R ~ 3.3, α is about 110.[21] Accordingly, we computed the shift of the plasmon resonance $\Delta\lambda_p$ upon variation of the dielectric constant $\Delta\varepsilon_m$ of the embedding medium ($\Delta\lambda_p$ (nm) = $\alpha\Delta\varepsilon_m$). Neglecting the weak absorption of the SCO compound, it can be readily shown that $\Delta\lambda_p$ (nm) ≈ α.2n.Δn where n is the average index of refraction of the SCO compound in the high spin and Δn the change of the index upon the spin state switching. We have previously shown that the index of refraction of SCO decreases upon switching of the SCO compounds from LS to HS states.[22] Hence, as already mentioned, the plasmon resonance should be blue shifted. Moreover according to our previous measurements and considering that n ~ 1.7 and 0.09 < Δn < 0.12,[22] a simple computation indicates that 33.6 nm < $\Delta\lambda_p$ < 44.9 nm in very good agreement with the experimental results.

2.7. Photoswitching properties

Since we aim at the synthesis of photoswitchable Au@SCO composites using low power irradiation, we performed photoswitching experiments using continuous-wave irradiation with a laser diode. It is worth mentioning that in a previous report, up to 2000 W/cm² (from a Raman spectrometer) was required to photoswitch SCO@SiO_2@Au composite compounds. [9] Our samples are prepared as for a classical photomagnetic measurement [23], which is a thin layer inserted inside a SQUID magnetometer sample holder. Before sending the laser beam on

the sample, three hysteretic cycles are recorded. This ensures the sample is well set within a stable hysteresis cycle. Let us mention that despite this caution, the switching temperature may slightly change by 1 or 2 degrees from one cycle to another. Prior to the experiment, the temperature of the sample is set in the LS state between 4 and 2 degrees below $T_{1/2}\uparrow$ (named ΔT_{exc}). Moreover, all the characterized samples, about 0.9 mg, are deposited on the same surface area (20 mm²) and shined with the same laser fluence of 15 mW/cm² of a 830 nm laser diode. The latter wavelength is close to the maximum of the longitudinal surface plasmon resonance band of the AuNRs and therefore should be strongly absorbed by the AuNRs imbedded in the SCO particles. The magnetization curves are recorded before irradiation and during the irradiation. After photo-saturation is reached, the laser is switched off and the temperature is decreased to recover the LS. The converted HS fraction is calculated as follows $(\chi_M T - (\chi_M T)_{t=0})/((\chi_M T)_{HS} - (\chi_M T)_{t=0})$, where $(\chi_M T)_{t=0}$ is the value of $\chi_M T$ just before the laser irradiation.

Figures 6 and **SI8-10** report the hysteresis curves of each compound together with the isothermal irradiation and the subsequent cooling curves. As displayed on figure 6 which compares compounds **1** and **5**, one can notice that laser irradiation does not impact the magnetization of compound **1** when $\Delta T_{exc} = 4$ K. However, $\chi_M T$ changes by about 15 % when the sample is stabilized 2 K below $T_{1/2}\uparrow$ indicating a partial LS to HS photoswitching. Similarly, compound **2** exhibits 15 % of photoswitching when $\Delta T_{exc} = 2$ K. In comparison, compound **3** is not sensitive to the applied light irradiation while compounds **4** and **5** are very sensitive to light irradiation. Indeed, compound **4** (**5**) shows 45% (55 %) of conversion when $\Delta T_{exc} = 2$ K. One should also mention that the photoswitching seems faster in nano-composites compared to sole SCO nanoparticles. Indeed, 90 % of the photoswitching is achieved in about 900 s in **5** compared to about 3600 s in **1**.

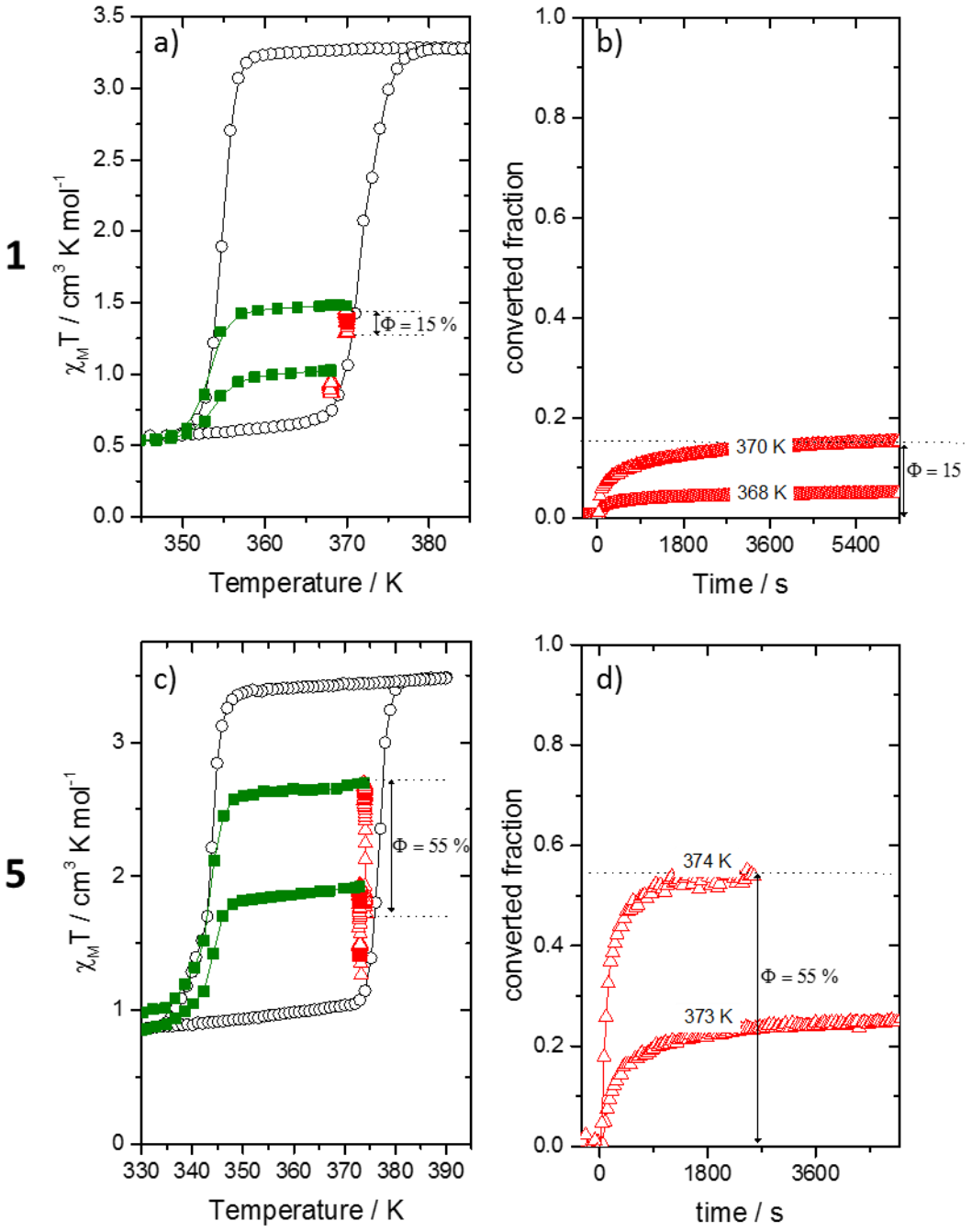

Figure 6: Photoswitching experiments performed on compounds **1** (top) and **5** (bottom), using a laser fluence of 15 mW/cm² centred at 830 nm. a) and c) report the hysteresis curve (o), the isothermal irradiations (Δ) and the following cooling curves (■). b) and d) report the converted HS fraction as function of time at two different temperatures.

Since the SCO compounds very weakly absorb in their HS state[22], these experiments evidence the strong enhancement of the photoswitching effect for AuNRs doped SCO NPs. The latter enhancement results from the activation of the AuNR nano heaters when the longitudinal SPR is excited. One should mention that a further reduction of the

photoswitching intensity may be achieved by centring the excitation of the laser wavelength on the maximum of the longitudinal SPR.

3. Conclusion

We have developed a synthesis protocol making possible to achieve in a reproducible and reliable way up to 90 % of Au@SCO core-shell nanoparticles of around 200 nm long. These nanocomposites exhibit several interesting and noticeable features. First, the AuNRs used seemed to bring a templating property during the synthesis of the composites, leading to well-defined architectures. Second, the Au@SCO nanoparticles exhibit hysteresis loops larger than pure SCO particles of similar size. Third, we have recorded a strong modulation of the SPR of the AuNRs upon the spin-state switching of the SCO shell. Within a temperature variation of 10 K, the SPR band, in the solid-state, is reversibly shifted by about 35 nm. Fourth, upon excitation of this SPR band by a low power laser beam, we have been able to photoswitch the SCO shell from the LS to the HS state of this Fe(II) complexes. This phenomenon results from the heating of AuNRs upon the excitation of their longitudinal SPR. The heat provided by these nano heaters is further transferred towards the SCO shell, inducing its efficient photoswitching. Even if the used wavelength was not well centred on the maximum of the longitudinal SPR, we succeeded in recording a drastic reduction of the fluence required to photoswitch the SCO shell compared to the pure SCO nanoparticles.

This work opens several interesting prospects. Among them, we would like to stress that since photoswitching of SCO nanoparticles can be achieved on a very short timescale (below 1 ns)[7], such hybrid materials may exhibit an ultrafast photoswitching of their surface plasmon resonance. With that regard, our nanomaterials bring new prospects with respect to the work recently published about the switching of plasmonic band in solid-state which results from reversible protonation/deprotonation of polymers grafted on silver nanoparticles.[24]

Moreover, one can foresee the use of such photoswitchable nanoparticles as a local probe of temperature at the nanometer scale.[8,25]

4. Experimental Section

Synthesis: The synthesis of $[Fe(Htrz)_2(trz)](BF_4)$ particles (**1**) using micellar method was done as reported in the literature[4f] using the following parameters: concentration of $Fe(BF_4)_2$ is fixed at 1.2 M and Tergitol NP-9 is chosen as surfactant (75%). The synthesis was performed at 50°C with a reaction time of 5 min. Concerning the direct synthesis of $[Fe(Htrz)_2(trz)](BF_4)$ (**2**), the same starting concentration of $Fe(BF_4)_2$ as the micellar synthesis was used but the volume used ofr the reaction was 1.7 mL of a H_2O/EtOH mixture (60/40) as well as for the 1*H*-1,2,4-triazole. Then both solutions were mixed at room temperature during 2h under magnetic stirring. The product is separated by centrifugation (8000 rcf, 5 min) and washed three times: the first with water and the last two ones with water/ethanol mixture. Finally, the $[Fe(Htrz)_2(trz)](BF_4)$ is let to dry overnight at ambient atmosphere. To synthesize hybrids Au@SCO (**3**, **4**, **5**), the AuNRs suspension was added to the Htrz solution, stirred for 1h to allow the Htrz to partially replace the outer layer of the CTAB surrounding the AuNRs and then the iron salt solution is added to this mixture. Same reaction steps as previously described were followed.

Powder X-Ray diffraction: Powder X-ray diffractogram are acquired using a PANalytical X'Pert^3 Powder (CuK, X'Celerator detector). More specifically the measurements were done using capillaries due to the small amount of compound that we have obtained. Measurements were done from 4 to 60 ° (2θ) using 60 s exposure with step of 0.017.

EDS analysis: EDS analysis were performed using a transmission electron microscope 2200 FS from JEOL (Japan) with a tension of 200 kV and a resolution of 1.9 Å in high resolution mode. EDS maps were done using a spot of 1.5 nm.

Transmission Electron Microscopy: Transmission electron microscopy (TEM) images are acquired using a JEOL 1400+ (Japan), with a high resolution mode and a tension of 60 kV. Each compound was analyzed separately and the measurements of 100 particles were done in order to give the average dimensions.

Magnetic and photomagnetic measurements were performed using a set of laser diodes coupled *via* an optical fibre to the cavity of a MPMS-5S Quantum Design SQUID magnetometer operating at 20 kOe. The powder sample was prepared in a thin layer (~0.9 mg on around 100 μm thickness) to promote full penetration of the light. The sample was weighted before any measurement and the diamagnetic contribution of the sample and the sample holder were removed. The thermal cycles were performed at around 0.7 K mn^{-1} scan rate. A laser diode delivering on the sample 15 mW cm^{-2} of fluence at 830 nm was used for all the measurements.

Optical characterisations:

The optical characterizations are carried out shining the sample with a high intensity fiber light source (Thorlabs OSL1-EC). At the exit of the fiber the light is collimated and then slightly focused on the sample. The light transmitted by the sample is then focused on the 600 µm input slit of the spectrometer (CVI CM110) equipped with a grating (1200 groove mm^{-1}) blazed at 600 nm. The diffracted light is transmitted by the 600 mm exit slit of the spectrometer and collected by a biased large area silicon photodiode (Thorlabs DET100A2).

Supporting Information

Supporting Information is available from the Wiley Online Library or from the author.

Acknowledgements: CNRS, University of Bordeaux, Nouvelle Aquitaine Region and the ANR program (HEROES ANR-17-CE09-0010-01) are acknowledged for fundings. The X-Ray diffraction facility of the ICMCB is also thanked for the powder diffraction experiments.

Received: ((will be filled in by the editorial staff))
Revised: ((will be filled in by the editorial staff))
Published online: ((will be filled in by the editorial staff))

References

[1] a) *Spin-Crossover Materials: Properties and Applications*, edited by M. A. Halcrow, 2013, John Wiley & Sons; b) S. Hayami, S. M. Holmes, M. A. Halcrow, *J. Mater. Chem. C* **2015**, *3*, 7775 and all included articles; c) P. Gütlich, A. B. Gaspar, Y. Garcia, *Beilstein J. Org. Chem.* **2013**, *9*, 342; d) A. Bousseksou, G. Molnár, L. Salmon, W. Nicolazzi, *Chem. Soc. Rev.* **2011**, *40*, 3313; e) K. S. Murray, H. Oshio, J. A. Real *Eur. J. Inorg. Chem.* **2013**, 577 and all included articles; (e) Eds. P. Gütlich and H. A. Goodwin, *Spin crossover in Transition Metal Compounds, Topics in Current Chemistry*, *Springer-Verlag Berlin Heidelberg NewYork* 2004, volumes I, II and III.

[2] (a) O. Kahn, C. Jay-Martinez, *Science* **1998**, *279*, 44; b) C. Lefter, V. Davesne, L. Salmon, G. Molnár, P. Demont, A. Rotaru, A. Bousseksou, *Magnetochem.* **2016**, *2*, 18; c) A. C. Aragonès, D. Aravena, J. I. Cerdá, Z. Acís-Castillo, H. Li, J. A. Real, F. Sanz, J. Hihath, E. Ruiz, I. Díez-Pérez, *Nano Lett.* **2016**, *16*, 218; d) F. Prins, M. Monrabal-Capilla , E. A. Osorio , E. Coronado, H. S. J. van der Zant, *Adv. Mater*. **2011**, *23*,1545; e) C. Lefter, R. Tan, S. Tricard, J. Dugay, G. Molnár, L. Salmon, J. Carrey, A. Rotaru, A. Bousseksou, *Polyhedron* **2015**, *102*, 434; f) X. Zhang, T. Palamarciuc, J.-F. Létard, P. Rosa, E. Vega Lozada, F. Torres, L. G. Rosa, B. Doudin, P. A. Dowben, *Chem. Commun*. **2014**, *50*, 2255; g) K. Senthil Kumar, M. Ruben, *Coord. Chem. Rev*. **2017**, *346*, 176; h) A. Bellec, J. Lagoute, V. Repain, *C. R. Chim*. **2012**, *21*, 1287

[3] a) P. N. Martinho, C. Rajnak, M. Ruben, *Spin-Crossover Materials: Properties and Applications*, 1st ed.; M. A. Halcrow, Ed.; John Wiley & Sons: City, UK, **2013**; pp. 375; b) A. Tissot, L. Rechignat, A. Bousseksou, M. L. Boillot, *J. Mater. Chem. C* **2012**, *22*, 3411; c) L. Salmon, L. Catala, *C. R. Chim*. **2018**, *21*, 1230

[4] a) E. Coronado, J. R. Galán-Mascarós, M. Monrabal-Capilla, J. Garciá-Martinez, P. Pardo-Ibañez, *Adv. Mater*. **2007**, *19*, 1359; b) T. Forestier, A. Kaiba, S. Pechev, D. Denux, P. Guionneau, C. Etrillard, N. Daro, E. Freysz, J.-F Létard, *Chem. Eur. J.* **2009**,

15, *6122*; c) D. Mader, S. Pillet, C. Carteret, M.-J Stébé, J.-L. Blin, *J. Dispers. Sci. Tech.* **2011**, *32*, 1771. d) I. A. Gural'skiy, C.M. Quintero, G. Molnár, I. O. Fritsky, L. Salmon, A. Bousseksou, *Chem. Eur. J.* **2012**, *18*, 9946; e) C. Bartual-Murgui, E. Natividad, O. Roubeau, *J. Mater. Chem. C*, **2015**, *3*, 7916; f) L. Moulet, N. Daro, C. Etrillard, J.-F Létard, A. Grosjean, P. Guionneau, *Magnetochem.* **2016**, *2(1)*, 10

[5] O. Roubeau, *Chem. Eur. J.* **2012**, *18*, 15230

[6] a) E. Freysz, S. Montant, S. Letard, J.-F. Létard, *Chem. Phys. Lett*. **2004**, *394*, 318; b) S. Bonhommeau, G. Molnar, A. Galet, A. Zwick, J. A. Real, J. J. McGarvey, A. Bousseksou, *Angew. Chem. Int. Ed.* **2005**, *44*, 2; c) S. Cobo, D. Ostrovskii, S. Bonhommeau, L. Vendier, G. Molnar, L. Salmon, K. Tanaka, A. Bousseksou, *J. Am. Chem. Soc.* **2008**, *130*, 9019; d) E. Collet, L. Henry, L. Piñeiro-López, L. Toupet, J. A. Real *Curr. Inorg. Chem*. **2016,** *6*, 61; e) F. Guillaume, Y.A. Tobon, S. Bonhommeau, J.-F. Létard, L. Moulet, E. Freysz, *Chem. Phys. Lett.* **2014**, *604*, 105.

[7] G. Gallé, C. Etrillard, J. Degert, F. Guillaume, J.-F. Létard, E. Freysz, *Appl. Phys. Lett.* **2013**, *102*, 063302.

[8] a) I. Suleimanov, O. Kraieva, J. Sanchez-Costa, I. O. Fritsky, G. Molnar, L. Salmon, A. Bousseksou, *J. Mater. Chem. C*. **2015**, *3*, 5026 ; b) I. Suleimanov, O. Kraieva, G. Molnar, L. Salmon, A. Bousseksou, *Chem. Commun*. **2015**, *51*, 15098.

[9] a) I. Suleimanov, J. Sanchez Costa, G. Molnar, L. Salmon, A. Bousseksou, *Chem. Commun*. **2014**, *50*, 13015; b) D. Qiu, L. Gu, X. -L. Sun, D. -H. Ren, Z.-G. Gu, Z. Lia, *R. Soc. Chem. Adv*. **2014**, 4, 61313.

[10] G. Baffou, R. Quidant, *Laser Photonics Rev*. **2013**, *7*, 171

[11] L. Moulet, N. Daro, S. Mornet, N. Vilar-Vidal, G. Chastanet, P. Guionneau, *Chem. Commun*. **2016**, *52*, 13213.

[12] B. Nikoobakht, M. A. El-Sayed, *Chem. Mater*. **2003**, *15*, 1957

[13] a) O. Kahn, J. Kröber, C. Jay, *Adv. Mater.* **1992**, *4*, 718 ; b) A. Michalowicz, J. Moscovici, B. Ducourant, D. Cracco, O. Kahn, *Chem. Mater*. **1995**, *7*, 1833.

[14] a) A. Grosjean, P. Négrier, P. Bordet, C. Etrillard, D. Mondieig, S. Pechev, E. Lebraud, J.-F. Létard, P. Guionneau, *Eur. J. Inorg. Chem.* **2013**, 796; b) A. Grosjean, N. Daro, S. Pechev, L. Moulet, C. Etrillard, G. Chastanet, P. Guionneau, *Eur. J. Inorg. Chem.* **2016**, 1961.

[15] N. Daro, PhD theses, University of Bordeaux, **2013.**

[16] L. P. Salamakha, E. Bauer, S. I. Mudryi, A. P. Goncalves, M. Almeida, H. Noel, *J. Alloys & Comp.* **2009**, *479*, 184.

[17] P. Gütlich, A. Hauser, H. Spiering, *Angew. Chem. Int. Ed. Engl*. **1994**, *33*, 2024.

[18] O. A. Yeshchenko, I. S. Bondarchuk, V. S. Gurin, I. M. Dmitruk, A. V. Kotko, *Surface. Science* **2013**, *608*, 275.

[19] R. Torres-Cavanillas, R. Sanchis-Gual, J. Dugay, M. Coronado-Puchau, M. Gimenez-Marques, E. Coronado, *Adv. Mater*. **2019**, *31*, 190039.

[20] K. Abdul-Kader, M. Lopes, C. Bartual-Murgui, O. Kraieva, E.M. Hernandez, L. Salmon, W. Nicolazzi, F. Carcenac, C. Thibault, G. Molnar, A. Bousseksou, *Nanoscale* **2013**, *5*, 5288.

[21] S. Link, M. B. Mohamed, M. A. El-Sayed, *J. Phys. Chem. B* **1999**, *103*, 3073.

[22] A. Iazzolino, G. Galle, J. Degert, J. F. Létard, E. Freysz, *Chem. Phys. Lett.* **2015**, *641*, 14.

[23] a) G. Chastanet, C. Desplanches, C. Baldé, P. Rosa, M.Marchivie and P. Guionneau, *Chem. Sq.* **2018**, *2*, 2; b) G. Chastanet, C. Desplanches, M. Gonidec, P. Guionneau, M. Marchivie, C. Mathoniere, P. Rosa, Elsevier,2019, ISBN 9780124095472, https://doi.org/10.1016/B978-0-12-409547-2.14646-3

[24] L. Liu, R. Aleisa, Y. Zhang, J. Feng, Y. Zheng, Y. Yin, W. Wang, *Angew. Chem. Int. Ed.* **2019**, *58*, 16307

[25] L. Salmon, G. Molnar, D. Zitouni, C. Quintero, C. Bergaud, J.-C. Micheau, A. Bousseksou, *J. Mater. Chem.* **2010**, *20*, 5499.

The synthesis of unprecedented gold@spin crossover (Au@SCO) nanocomposites is reported. They exhibit a strong interplay between surface plasmon resonance (SPR) and spin state switching. The spin state change induces a 35 nm modulation of the longitudinal SPR of the gold core. The latter acts as a local nanoheater to enhance the photothermal effect and the subsequent photo-induced SCO.

Keywords: Spin crossover, surface plasmon resonance, gold nanoparticle, photoswitching, SPR modulation

Marlène Palluel, Ngoc Minh Tran, Nathalie Daro, Sonia Buffière, Stéphane Mornet,* Eric Freysz* and Guillaume Chastanet*

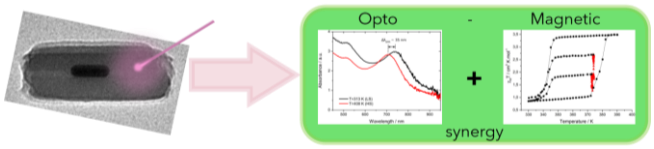

Supporting information

The Synergy between Surface Plasmon Resonance and Switching Properties in Gold@Spin Crossover Nano-Composites

Marlène Palluel, Ngoc Minh Tran, Nathalie Daro, Sonia Buffière, Stéphane Mornet,* Eric Freysz* and Guillaume Chastanet*

Content:

Figure SI1: *a) TEM image of gold nanorods and b) the histograms of their sizes. The lines stand for the gaussian fit of these histograms.*

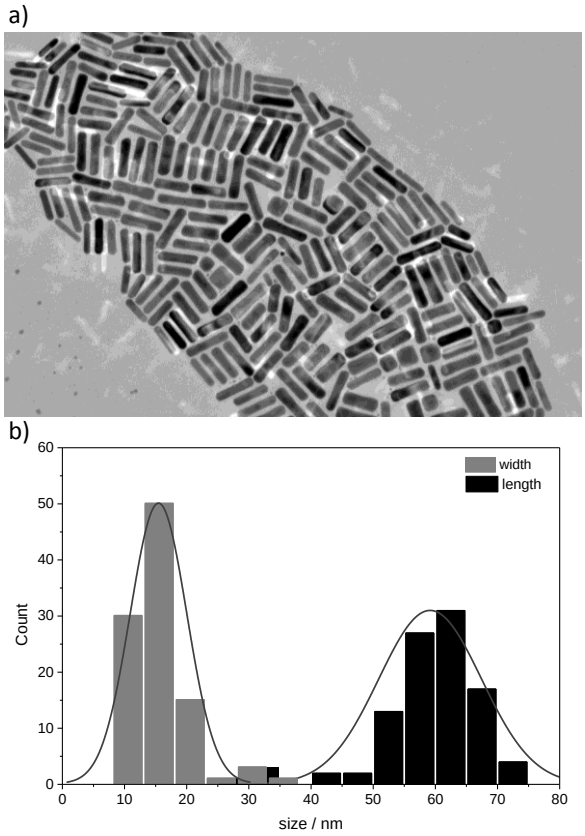

Figure SI2: *picture of destabilized and stabilized gold microemulsion.*

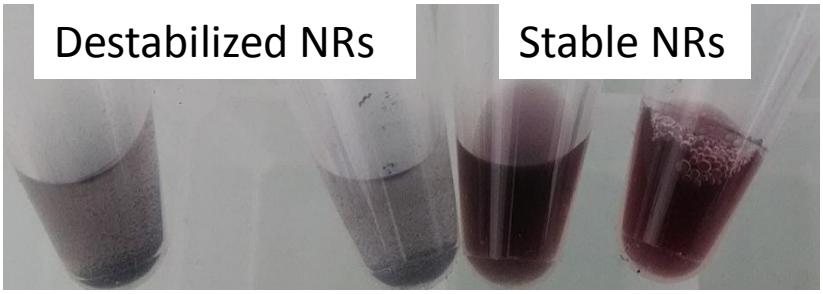

Table SI1*: Stability tests of the colloidal suspension of the gold nanorods into a mixture of EtOH and water, after few minutes of incubation. This stability is evaluated by eyes: a stable suspension being burgundy colored while a destabilized suspension is uncolored with black precipitated particles. The stability is noted "++" for the best to "- - " for the worst. All volume are in µL.*

V(EtOH) / µL	0	20	40	60	80
V(Au in H_2O)* / µL	20	20	20	20	20
V(H_2O) / µL	80	60	40	20	0
Stability	++	++	+	--	--

* V(Au in H_2O) is the volume of the gold nanorods suspension obtained after synthesis in water and stabilized by 5 mM of CTAB.

Table SI2*: Stability tests of Au – Htrz dispersion in a mixture of H_2O/EtOH by varying the concentration of Htrz of the dispersion <u>after 0 h of incubation</u>. This stability is evaluated by eyes: a stable suspension being burgundy colored while a destabilized suspension is uncolored with black precipitated particles (cf Figure SI2). The stability is noted "++" for the best to "- - " for the worst. All volume presented are in µL.*

V(EtOH)	0	20	40	60	80
V(Au – Htrz in H_2O)	20	20	20	20	20
V(H_2O)	80	60	40	20	0
[Htrz]	Stability				
100 mM	++	++	-	--	--
200 mM	++	++	~	--	--
300 mM	++	++	~	--	--
400 mM	++	++	-	--	--
500 mM	++	++	+	--	--
1 M	++	++	~	--	--
1.5 M	++	++	-	--	--
1.8 M			+		
2 M	++	++	-	--	--

Figure SI3: *Images of stability tests corresponding to Table SI2. From 0 µL of EtOH on the left to 80 µL of EtOH on the right.*

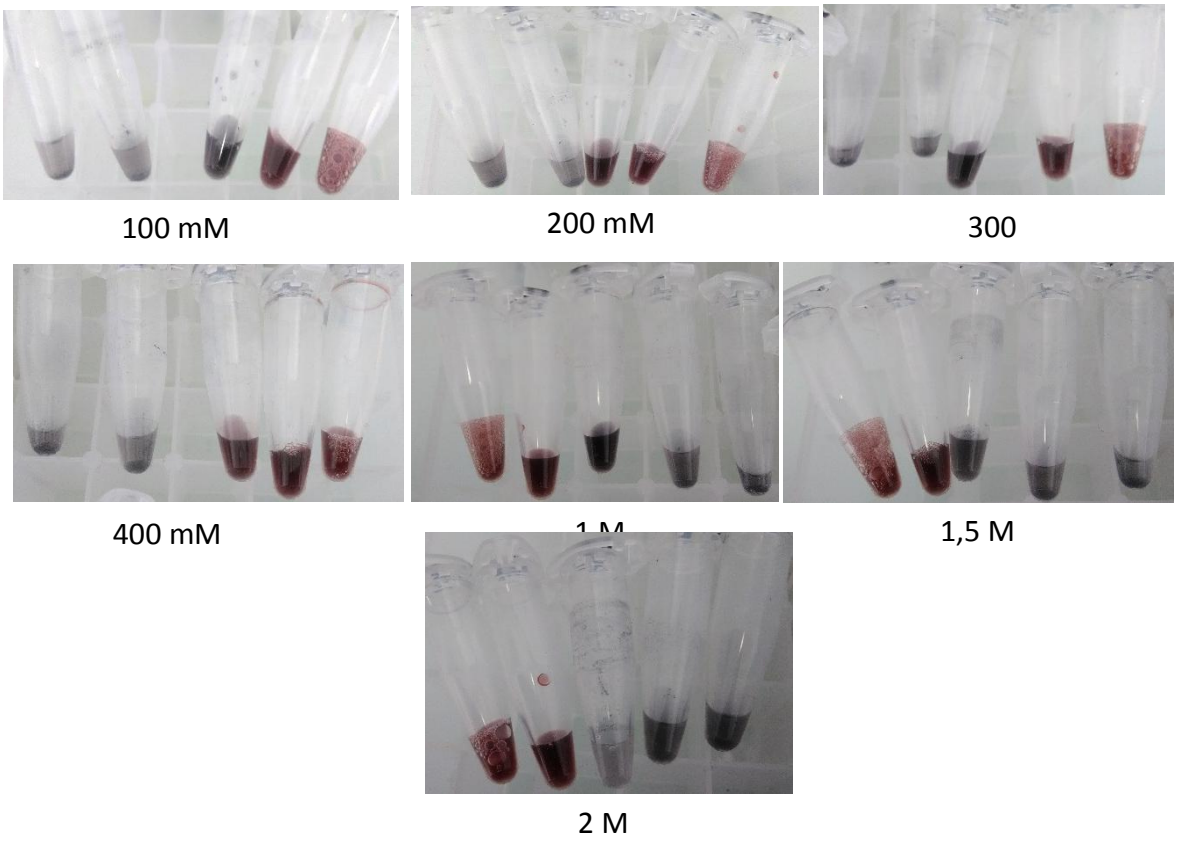

Table SI3: *Stability tests of Au – Htrz dispersion in a mixture of H_2O/EtOH by varying the concentration of Htrz after 1h (in black) and 24 h (in red) of incubation. This stability is evaluated by eyes: a stable suspension being burgundy colored while a destabilized suspension is uncolored with black precipitated particles. The stability is noted "++" for the best to "- - " for the worst. All volume presented are in µL.*

V(EtOH)	20	25	30	35	40	45	50	55	60
V(Au – Htrz in H_2O)	20	20	20	20	20	20	20	20	20
V(H_2O)	60	55	50	45	40	35	30	25	20
[Htrz]	Stability								
100 mM	++	++	++ / ++	++ / ++	+ / +	-- / --	-- / --		
200 mM			++ / ++	++ / ++	+ / +	-- / --	-- / --		
300 mM			++	++	- / -	-- / --	-- / --		
400 mM			++ / ++	++ / ++	+ / +	-- / --	-- / --	--	--
500 mM					+ / +	-- / --	-- / --	-- / --	-- / --
1 M			++ / ++	++ / ++	~ / -	-- / --	-- / --		
1.5 M	++	++	++ / ++	++ / ++	~ / ~	-- / --	-- / --		
1.8 M					+ / +				
2 M	++	++	++ / ++	++ / ++	~ / -	-- / --	-- / --		

Figure SI4: *TEM image of compound **3**. Gold nanorods are evidenced by the red circles.*

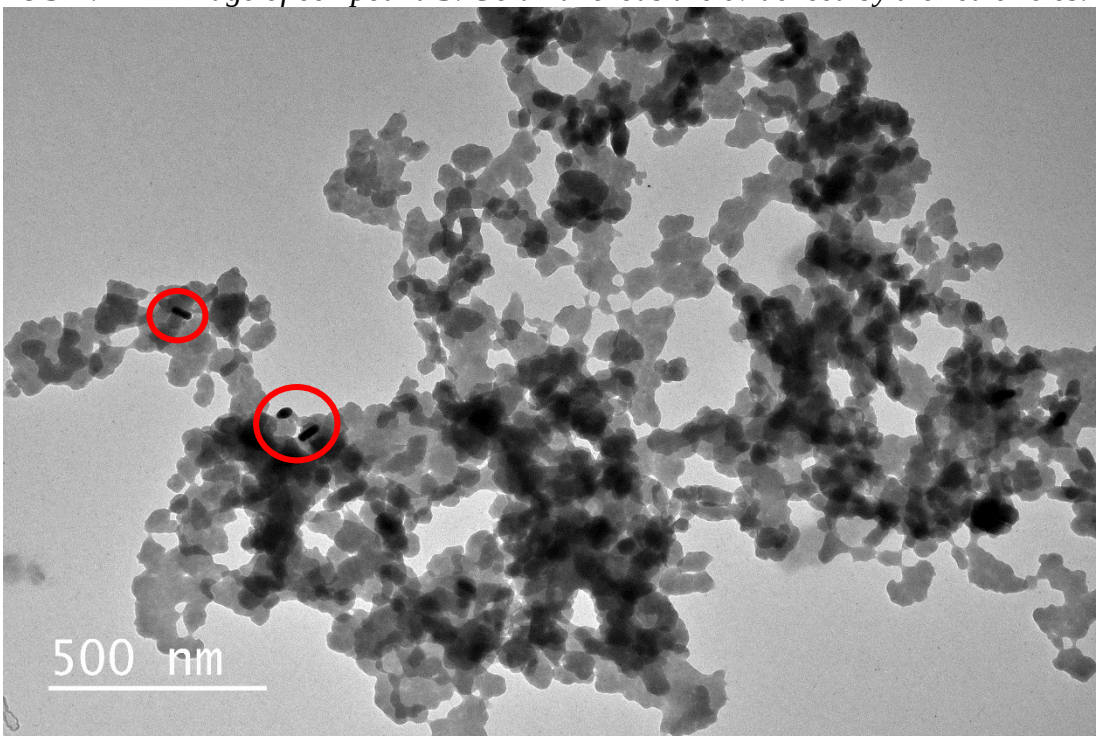

Figure SI5: *EDS images of **4**.*

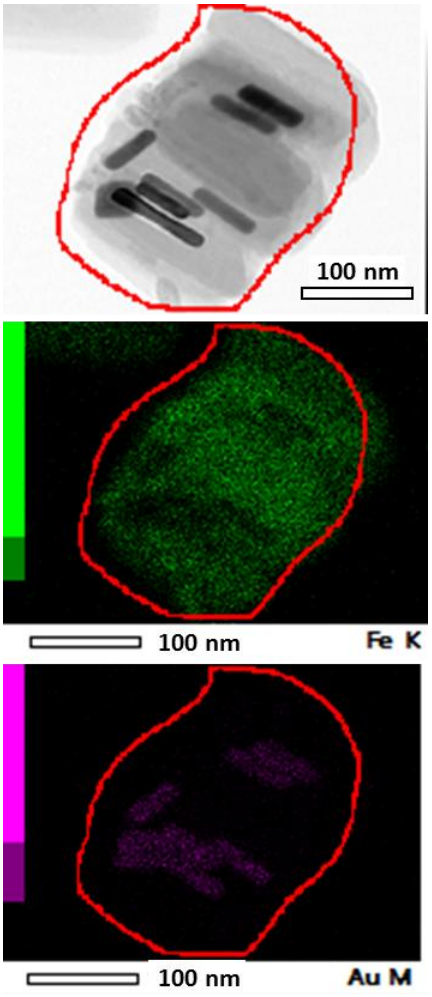

Figure SI6: *Thermal dependence of the absorption spectra of **1**.*

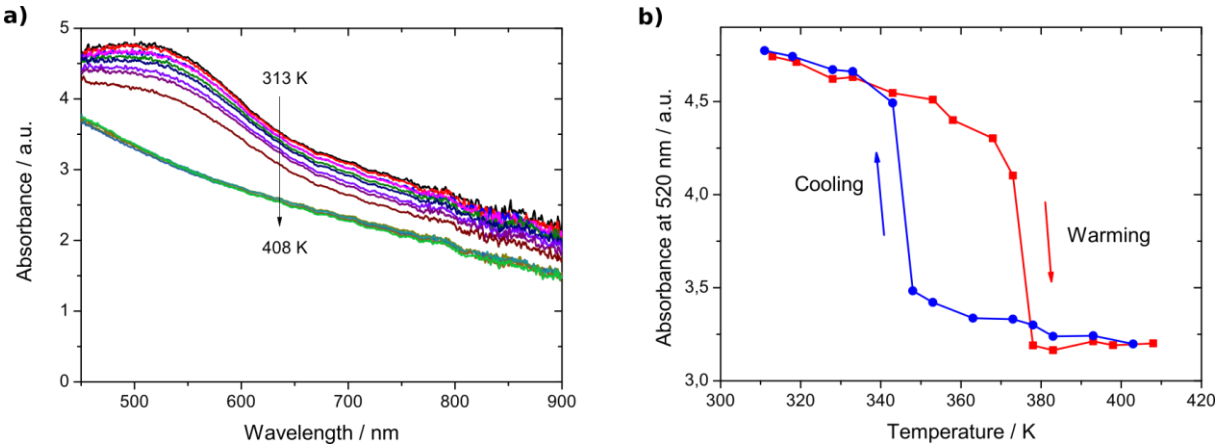

Figure SI7: *Thermal dependence of the absorption spectra of **4**.*

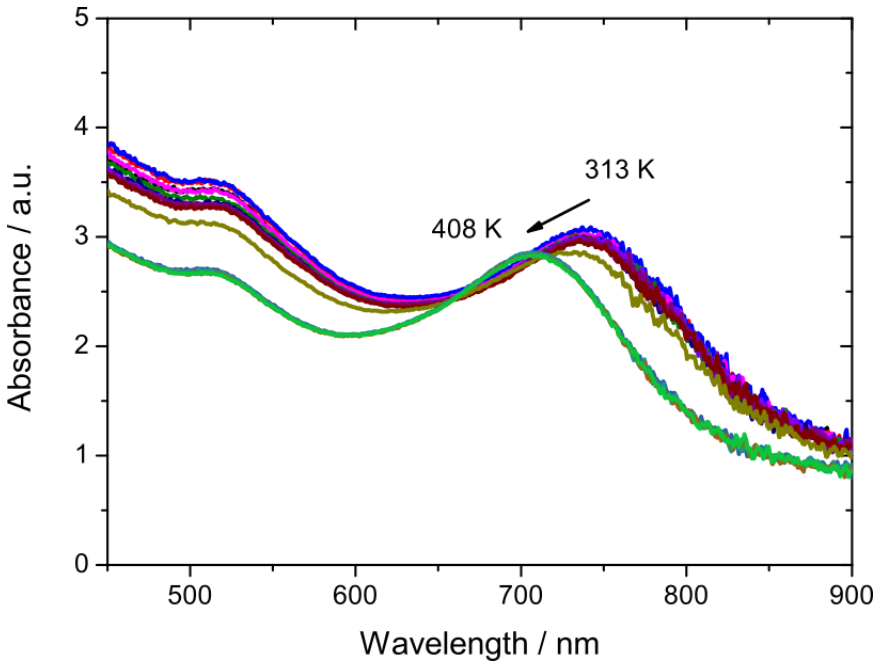

Figure SI8: *Thermal evolution of the $\chi_M T$ product of **2** upon thermal cycling and irradiation of the sample using a 830 nm wavelength at 15 mW/cm^2.*

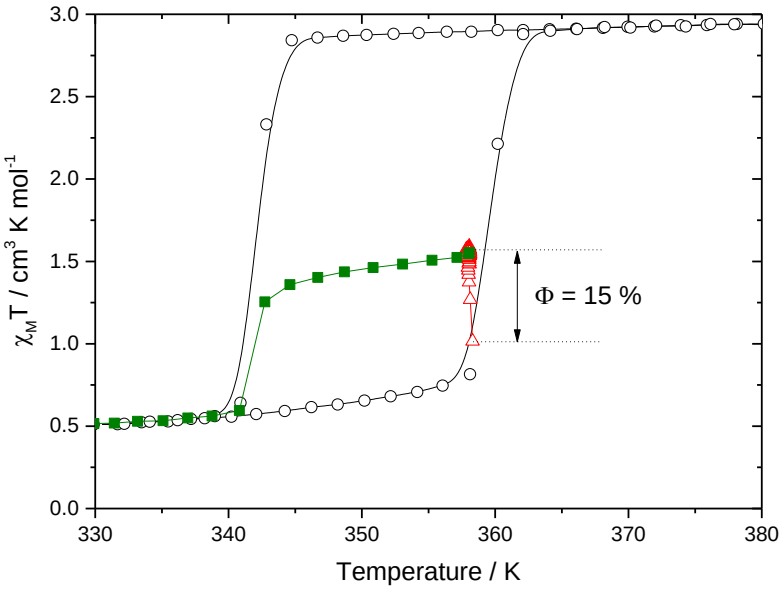

Figure SI9: *Thermal evolution of the $\chi_M T$ product of **3** upon thermal cycling and irradiation of the sample using a 830 nm wavelength at 15 mW/cm^2.*

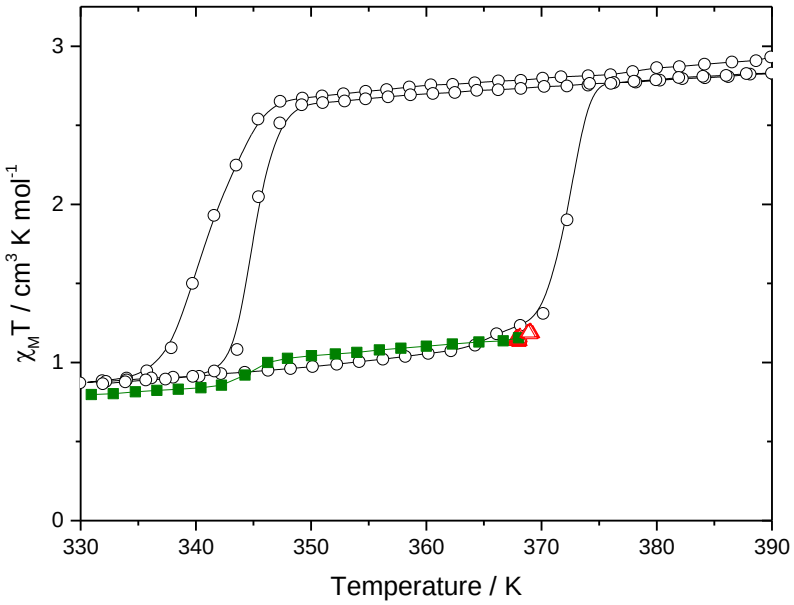

Figure SI10: *Thermal evolution of the $\chi_M T$ product of **4** upon thermal cycling and irradiation of the sample using a 830 nm wavelength at 15 mW/cm^2.*